

# Photoionization-cross-section measurement of the $^{85}\text{Rb } 5^2\text{P}_{3/2}$ excited state using microwave cavity resonance spectroscopy

**Citation for published version (APA):**

van Nijnhuijs, M. A. W., Beckers, J., & Luiten, O. J. (2022). Photoionization-cross-section measurement of the  $^{85}\text{Rb } 5^2\text{P}_{3/2}$  excited state using microwave cavity resonance spectroscopy. *Physical Review A*, 106(6), Article 063110. <https://doi.org/10.1103/PhysRevA.106.063110>

**DOI:**

[10.1103/PhysRevA.106.063110](https://doi.org/10.1103/PhysRevA.106.063110)

**Document status and date:**

Published: 23/12/2022

**Document Version:**

Publisher's PDF, also known as Version of Record (includes final page, issue and volume numbers)

**Please check the document version of this publication:**

- A submitted manuscript is the version of the article upon submission and before peer-review. There can be important differences between the submitted version and the official published version of record. People interested in the research are advised to contact the author for the final version of the publication, or visit the DOI to the publisher's website.
- The final author version and the galley proof are versions of the publication after peer review.
- The final published version features the final layout of the paper including the volume, issue and page numbers.

[Link to publication](#)

**General rights**

Copyright and moral rights for the publications made accessible in the public portal are retained by the authors and/or other copyright owners and it is a condition of accessing publications that users recognise and abide by the legal requirements associated with these rights.

- Users may download and print one copy of any publication from the public portal for the purpose of private study or research.
- You may not further distribute the material or use it for any profit-making activity or commercial gain
- You may freely distribute the URL identifying the publication in the public portal.

If the publication is distributed under the terms of Article 25fa of the Dutch Copyright Act, indicated by the "Taverne" license above, please follow below link for the End User Agreement:

[www.tue.nl/taverne](http://www.tue.nl/taverne)




**Take down policy**

If you believe that this document breaches copyright please contact us at:

[openaccess@tue.nl](mailto:openaccess@tue.nl)

providing details and we will investigate your claim.

## Photoionization-cross-section measurement of the $^{85}\text{Rb } 5^2P_{3/2}$ excited state using microwave cavity resonance spectroscopy

M. A. W. van Nihuijs , J. Beckers , and O. J. Luiten \*

*Department of Applied Physics, Eindhoven University of Technology, P.O. Box 513, 5600 MB Eindhoven, The Netherlands*



(Received 4 August 2022; accepted 21 November 2022; published 23 December 2022)

We present microwave cavity resonance spectroscopy as a technique to determine excited-state photoionization cross sections of laser-cooled atoms. We demonstrate this technique by measuring the photoionization cross section of the  $5^2P_{3/2}(F' = 4)$  excited state of  $^{85}\text{Rb}$  to continuum by creating an ultracold plasma inside a 5-GHz resonant microwave cavity. We find a photoionization cross section of  $\sim 5 \times 10^{-22} \text{ m}^2$  for photon excess energies of 50, 100, 200, and 500 K above the ionization threshold. The measurements yield a cross section which is approximately 2 to 3 times smaller than the value provided by existing theory for the  $5p$  excited state of  $^{85}\text{Rb}$  and two earlier measurements performed with other techniques for similar excess energies.

DOI: [10.1103/PhysRevA.106.063110](https://doi.org/10.1103/PhysRevA.106.063110)

### I. INTRODUCTION

Photoionization cross sections determine the probability that an atom is ionized by one or more photons; they are of fundamental importance for the understanding of many types of plasmas, such as astrophysical plasmas [1], controlled thermonuclear plasmas [2], and plasmas induced by extreme ultraviolet irradiation in state-of-the-art photolithography tools [3], and for the production of laser-produced plasmas such as the ultracold plasma (UCP) [4] described in this paper.

For atoms that are photoionized in a two-step photoionization process, a few experimental techniques have been developed over the last couple of decades to measure their photoionization cross section from the excited state to the continuum. These techniques include the use of a magneto-optical trap (MOT) [5] and the saturation technique [6]. In the first technique, atom losses from the MOT by photoionization are taken into account as an additional loss term in the rate equations that describe the loading process of atoms in the trap [7]. By measuring the increase (decrease) of the fluorescence signal of atoms in the excited state, the photoionization cross section can be determined.

The saturation technique uses an excitation laser beam that is operated at intensities higher than the saturation intensity to create an equilibrium with half of the population of atoms in the excited state and half in the ground state. Subsequently, the atoms in the excited state are photoionized with a pulsed ionization laser with a pulse length that is short compared to the lifetime of the excited state to prevent excited atoms from decaying to the ground state. By measuring the number of ions created as a function of the ionization-laser-pulse energy and increasing the pulse energy until the ionization laser beam transition is saturated as well, the photoionization cross section can be determined from curve fitting the measured data

with an exponential fit function. This method allows the cross section to be determined without having to know the exact number of atoms present before photoionization, as we will see later.

The number of ions created in the two-step photoionization process using the saturation technique can be determined in a few different ways [1]. For example, Ambartzumian *et al.* used two parallel capacitor plates, one held at ground and the other at a negative potential, in order to collect the ions created from the photoionization of a metallic vapor between the capacitor plates [6]. Kallenbach *et al.* used a setup with a thermionic diode, in which its cathode was heated [8]. This results in the thermionic emission of electrons from the cathode and creates a negatively charged region in its vicinity. By subsequently photoionizing a metallic vapor of interest in the setup, some of the emitted electrons are neutralized by the created ions. This results in an increase of the diode current, which can be used as a measure for the number of ions created. A third technique that is being employed is a triple-crossed-beam apparatus, in which two lasers used for photoionization intersect with a collimated beam from an atomic oven [9]. The ions created in the overlap volume of the lasers and atomic beam can be extracted by a small electric field applied between two electric grids around the overlap volume. By accelerating the ions towards a particle detector with the field, the number of ions in the experiment can be determined. If the ions are, after extraction, additionally accelerated with a higher electric field in combination with a drift space, then such a setup can also be used as a time-of-flight mass spectrometer [10]; this allows the photoionization cross section of different isotopes of an atomic species to be determined since ions with a different isotopic mass will arrive at a different time at the ion detector.

In this paper, we present *microwave cavity resonance spectroscopy* (MCRS) as a technique to determine the photoionization cross section. We give a proof of concept of this technique by measuring the photoionization cross section of the  $5^2P_{3/2}(F' = 4)$  excited state of  $^{85}\text{Rb}$  using the saturation technique in combination with a 5-GHz resonant microwave

\*o.j.luiten@tue.nl

cavity as a charged-particle detector. For this, we first laser cool and trap a cloud of  $^{85}\text{Rb}$  atoms in a compact magneto-optical trap, using a diffraction grating chip [11,12] inside a microwave cavity, and subsequently we photoionize the atoms in a two-step photoionization process. By using a saturating excitation laser pulse we excite half of the atomic population of the  $5^2S_{1/2}(F=3)$  ground state to the  $5^2P_{3/2}(F'=4)$  excited state and subsequently photoionize the atoms just above threshold with a nanosecond pulsed dye laser in order to create an ultracold plasma. By measuring the shift in the resonance frequency of the cavity, induced by the ultracold plasma, we obtain a measure for the number of electrons present in the plasma immediately after photoionization and thus for the number of ions as well (since the atoms are singly ionized). Repeating this measurement for different pulse energies of the photoionization laser until the ionization transition is saturated too therefore enables us to determine the photoionization cross section of the excited state of  $^{85}\text{Rb}$ .

The outline of this paper is as follows. In Sec. II, we briefly review the theory of the saturation technique. By using rate equations for the three levels involved in a two-step photoionization process, we derive an expression for the number of ions created during this process, which can be used to determine the photoionization cross section from the excited state. Subsequently, in Sec. III, we discuss the experimental setup and how our microwave cavity can be used to obtain the cross section of the  $5^2P_{3/2}(F'=4)$  excited state of  $^{85}\text{Rb}$ . We then show, in Sec. IV, the results of a measurement of the photoionization cross section for four different wavelengths of the ionization laser beam and compare them to theoretical predictions and a few earlier measurements performed by other groups (Sec. V). Finally, we end with some concluding remarks and an outlook for further developments.

## II. THEORY

Consider a three-level system consisting of a ground state, an excited state, and an ionized state. The particle number density of the atoms in the ground state is given by  $n_1$ , the number density in the excited state is given by  $n_2$ , and the number density in the ionized state is given by  $n_i$ . When an excitation laser is used to optically pump the atoms from the ground state to the excited state and an ionization laser is used to photoionize the atoms near threshold, the change in the particle number densities as a function of time  $t$  for each of the states is governed by the following rate equations [1,13]:

$$\frac{dn_1(t)}{dt} = -R_{\text{abs}}(t)[n_1(t) - n_2(t)], \quad (1a)$$

$$\frac{dn_2(t)}{dt} = R_{\text{abs}}(t)[n_1(t) - n_2(t)] - R_{\text{pi}}(t)n_2(t), \quad (1b)$$

$$\frac{dn_i(t)}{dt} = R_{\text{pi}}(t)n_2(t). \quad (1c)$$

Here,  $R_{\text{abs}}(t)$  is the photoabsorption rate, and  $R_{\text{pi}}(t) = \sigma_{\text{pi}}I_{\text{pi}}(t)/E_{\text{ph}}$  is the photoionization rate, with  $\sigma_{\text{pi}}$  being the photoionization cross section from the excited state to continuum,  $I_{\text{pi}}(t)$  being the intensity of the photoionization laser, and  $E_{\text{ph}} = hc/\lambda$  being the photon energy, where  $\lambda$  is the wave-

length of the photoionization laser,  $h$  is Planck's constant, and  $c$  is the speed of light.

In the saturation technique, we furthermore assume that the excitation transition is fully saturated, such that approximately half of the total atomic number density  $n_{\text{tot}}(t) \equiv n_1(t) + n_2(t)$  is in the excited state, i.e.,

$$n_2(t) \approx n_{\text{tot}}(t)/2. \quad (2)$$

Using this fact and adding Eq. (1a) to Eq. (1b) results in the following differential equation for the excited-state density:

$$\frac{dn_2(t)}{dt} = -\frac{1}{2}R_{\text{pi}}(t)n_2(t). \quad (3)$$

Integrating Eq. (3) and using the initial condition  $n_2(0) = n_{\text{tot}}(0)/2$  give the solution for the excited-state density:

$$n_2(t) = \frac{1}{2}n_{\text{tot}}(0) \exp\left(-\frac{1}{2} \int_0^t R_{\text{pi}}(\tilde{t})d\tilde{t}\right). \quad (4)$$

Suppose the ionization laser pulse, with pulse length  $\tau$ , starts to photoionize the excited atoms at time  $t = 0$ . The ion density at time  $t = \tau$  can then be found by substituting Eq. (4) into Eq. (1c) and integrating over the ionization-laser-pulse length  $\tau$ , which gives

$$\begin{aligned} n_i(\tau) &= \int_0^\tau R_{\text{pi}}(t)n_2(t)dt \\ &= \frac{1}{2}n_{\text{tot}}(0) \int_0^\tau R_{\text{pi}}(t) \exp\left(-\frac{1}{2} \int_0^t R_{\text{pi}}(\tilde{t})d\tilde{t}\right)dt. \end{aligned} \quad (5)$$

Equation (5) can be evaluated by integration by substitution and by substituting the definition of the photoionization rate  $R_{\text{pi}}$  into Eq. (5). The particle number density  $n_i$  of ions created in the two-step photoionization process then becomes [14]

$$n_i(\tau) = n_{\text{tot}}(0) \left[ 1 - \exp\left(-\frac{\sigma_{\text{pi}}F}{2E_{\text{ph}}}\right) \right], \quad (6)$$

with

$$F = \int_0^\tau I_{\text{pi}}(\tilde{t})d\tilde{t} \quad (7)$$

being the fluence (energy per area) of the ionization laser pulse.

If we furthermore assume that the photoionization laser beam has a constant fluence  $F = E_{\text{pulse}}/A$  in the overlap volume of the atoms with the excitation laser beam and ionization laser beam, with  $E_{\text{pulse}}$  and  $A$  being the ionization-laser-pulse energy and beam area, respectively, then the number of ions  $N_i$  created in the two-step photoionization process follows from simply multiplying the ion density in Eq. (6) by the overlap volume  $V$ . Hence,

$$N_i = N_{\text{tot}}(0) \left[ 1 - \exp\left(-\frac{\sigma_{\text{pi}}F}{2E_{\text{ph}}}\right) \right], \quad (8)$$

with  $N_{\text{tot}}(0) = n_{\text{tot}}(0)V$  being the total of number of atoms at time  $t = 0$ .

Equation (8) is typically used as a fit function to determine the photoionization cross section with the saturation technique; by measuring the number of ions created as a function of the ionization-laser-pulse energy, until the ionization transition is saturated too, the photoionization cross section can be

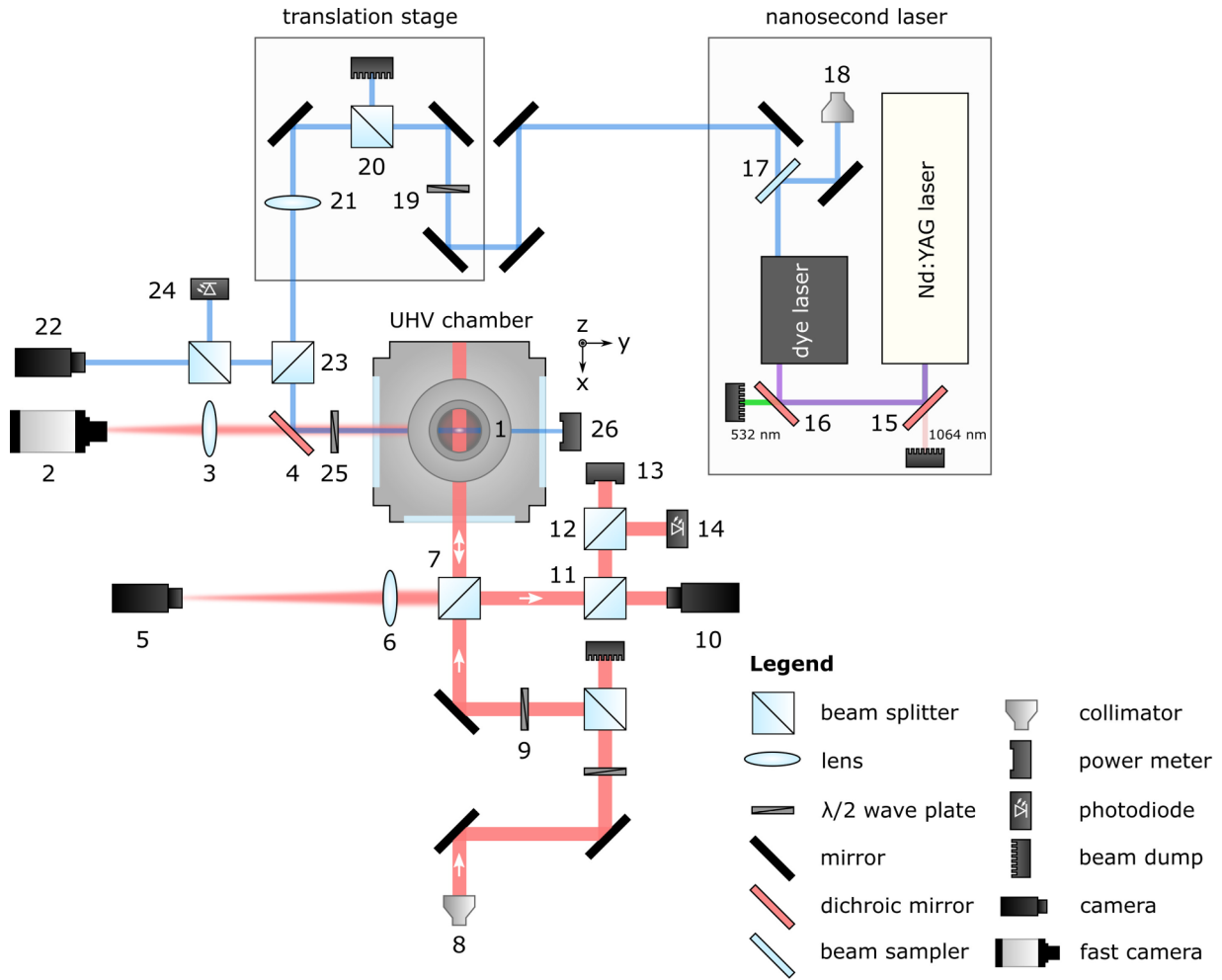


FIG. 1. Experimental setup with the nanosecond ionization laser, laser translation stage, ultrahigh vacuum chamber containing the resonant microwave cavity (1), and several other parts; a complete description of the setup is given in the text.

obtained from fitting the measured data with this exponential function.

The advantage of using Eq. (8) as a fit function is that an accurate determination of the photoionization cross section requires only the wavelength  $\lambda$  of the ionization laser and its beam area in the overlap volume of the lasers and atoms to be measured; it does not require knowledge of the total number of atoms present before photoionization since the exponential behavior of Eq. (8) makes the total number of atoms a fit parameter as well.

However, in reality, the ionization laser often does not have a constant fluence in the overlap volume but has a Gaussian shape, in which the tails of the Gaussian profile can contribute considerably to the production of ions [15]. This is also true for the experiment performed in this paper, and we therefore use an adapted version of Eq. (8), which takes the spatial profile of the ionization laser beam into account. In Sec. III, we will discuss this in more detail, together with how the frequency shift in the cavity, induced by an ultracold plasma, can be used as a measure for the number of ions present in the plasma.

### III. EXPERIMENT AND METHODS

#### A. Optical setup

The setup used for the determination of the photoionization cross section of  $^{85}\text{Rb}$  is depicted in Fig. 1. The main part consists of an ultrahigh vacuum (UHV) chamber with a microwave cavity inside (labeled 1) in which a cloud of  $^{85}\text{Rb}$  atoms is laser cooled and trapped using a grating chip MOT, as discussed in previous papers [16,17]. This is done with a 780-nm cooling laser, which drives the  $5^2S_{1/2}(F=3)$  to  $5^2P_{3/2}(F'=4)$  cooling transition nonresonantly and which enters the cavity through the hole shown in Fig. 1. The laser also contains sidebands added with an electro-optic modulator to drive the  $5^2S_{1/2}(F=2)$  to  $5^2P_{3/2}(F'=3)$  repump transition to prevent losses of atoms to the  $5^2S_{1/2}(F=2)$  ground state. To count the number of atoms present in the magneto-optical trap and to determine the atomic density profile, two infrared cameras are used to image the fluorescence of the  $5^2P_{3/2}$  excited state to the  $5^2S_{1/2}$  ground state: one fast camera (2) with a zoom lens (3) positioned behind a dichroic mirror (4) and another camera (5) with a lens (6) that makes a

one-to-one image of the ultracold atoms from a perpendicular angle through a 50:50 nonpolarizing beam splitter (BS) cube (7).

After the magneto-optical trap has been loaded with atoms, an ultracold plasma is created by two-step photoionization. The trapping laser is rapidly turned off with an acousto-optic modulator to let the atoms in the excited state decay to the  $5^2S_{1/2}$  ground state. After 1  $\mu$ s (which is much longer than the 26-ns lifetime of the excited state), the excitation laser beam is turned on to resonantly excite the atoms to the  $5^2P_{3/2}$  state. The excitation laser beam, which is fiber coupled, is split off from the trapping laser beam (not shown here) and enters the setup through a collimator (8). It has a Gaussian rms size of  $3 \times 10^2 \mu\text{m}$ ; is linearly polarized, with its angle of polarization set by a  $\lambda/2$  wave plate (9); and has a typical power of 1.3 mW upon arrival in the cavity. As a result, the beam has a peak intensity  $I_0 = 1.3/[2\pi \times (0.03)^2] = 2 \times 10^2 \text{ mW/cm}^2$ , which is much larger than the saturation intensity  $I_{\text{sat}} = 3.12950 \text{ mW/cm}^2$  for  $\pi$ -polarized light for the  $5^2S_{1/2}(F=3)$  to  $5^2P_{3/2}(F'=4)$  cycling transition [18]. This results in an on-resonance saturation parameter  $s_0 = I_0/I_{\text{sat}} = 7 \times 10^1$ , and the steady-state excited-state fraction  $f_2$  will therefore be  $f_2 = \frac{1}{2}s_0/(1+s_0) \approx \frac{1}{2}$ , which justifies the use of the saturation technique.

The excitation laser is operated in both pulsed and continuous-wave (cw) modes. The pulsed mode is used for performing the measurements of the photoionization cross section. An excitation pulse with a pulse length of 3  $\mu$ s is used, which is more than enough for the atoms to reach the steady-state situation in which half of the atoms occupy the excited state. In between measurements, when the pulse energy of the photoionization laser is changed, the excitation laser is switched to the cw mode in order to monitor the beam profile and laser power since the energy in a single excitation laser pulse is not large enough to measure. Monitoring is done to ensure the laser power is large enough for the excitation transition to be saturated. To capture the beam profile, an infrared camera (10) is placed at an optical path length from the 50:50 BS cube (7), which is the same as the path length from the 50:50 BS cube to the center of the cavity. The camera is placed behind a 58:42 nonpolarizing BS cube (11), which transmits 58% of the light in the forward direction. The remaining 42% is split off and subsequently divided by another nonpolarizing beam splitter (12); 50% of the light is directed to a power meter (13), and 50% is measured with a fast photodiode detector (14). The latter is used to temporally overlap the excitation laser pulse with the photoionization laser pulse in the cavity on an oscilloscope.

After being excited to the  $5^2P_{3/2}$  state, the atoms are ionized with a nanosecond photoionization laser. The nanosecond photoionization laser setup consists of a 1064-nm Q-switched Nd:yttrium aluminum garnet (YAG) laser used to pump a 480-nm tunable pulsed dye laser at a repetition rate of 10 Hz; the Nd:YAG laser has two crystals on its output side, used for second-harmonic generation (532 nm) and sum-frequency generation (355 nm). Two dichroic mirrors (15 and 16) are used to filter out the 1064- and 532-nm components, and the remaining 355-nm pulses are subsequently used to pump a dye of Coumarin 480 in the dye laser in order to generate 480-nm nanosecond laser pulses. The exact wavelength of the dye

laser pulses is set by the angle of a diffraction grating inside the dye laser and is monitored throughout the experiment with a Fizeau interferometric wavemeter by splitting off 1% of the output beam power with a beam sampler (17) and coupling the light into a collimator (18) connected to the wavemeter. The pulses have a Gaussian beam profile with an rms size of 1.1 by 0.8  $\text{mm}^2$  in the  $x$  and  $z$  directions, respectively (see Fig. 1), and a pulse energy up to  $\sim 500 \mu\text{J}$  upon arrival in the cavity, with a FWHM pulse length of 6 ns. The dye laser pulses photoionize the atoms with a delay of 250 ns with respect to the start of the excitation laser pulse in order to let the atoms obtain a steady-state excited-state fraction  $f_2 \approx \frac{1}{2}$  before photoionization.

A computer-controlled translation stage steers the ionization laser beam in the  $xz$  plane of the cavity (see Fig. 1), which simplifies overlapping the ionization laser beam with the excitation laser beam considerably, without having to manually adjust the angles of several mirrors in the optical path before the cavity. The stage also contains a computer-controlled  $\lambda/2$  wave plate (19) in front of a polarizing BS cube (20) which can be used to control the pulse energy of the ionization laser beam by changing the angle of the wave plate.

The ionization laser beam is focused towards the cavity with a lens (21) attached to the translation stage, and its beam profile is measured with a camera (22). The camera was placed behind a 90:10 nonpolarizing BS cube (23) at a distance that is the same as the optical path length from the nonpolarizing BS cube to the center of the cavity. This was done in order to measure the size of the ionization laser beam, which is crucial for the correct determination of the photoionization cross section. A fast photodiode detector (24) is used in combination with another fast photodiode detector (14) to temporally overlap the ionization laser with the excitation laser beam. A computer-controlled  $\lambda/2$  wave plate (25) in front of the UHV chamber is used to change the angle of the linearly polarized ionization laser beam, and a power meter (26) behind the UHV chamber measures the pulse energy of the nanosecond laser pulses. Since the UV-grade fused silica windows of the UHV chamber transmit only 92% of the light at 480 nm, we correct for the decrease in pulse energy arriving at the power meter in the analysis.

In order to spatially overlap the excitation laser beam with the ionization laser beam and the ultracold atomic cloud, the following procedure was followed. First, the trapping laser beam was kept on all the time, and the ionization laser beam was moved in the  $xz$  plane with the translation stage until the laser overlapped with the laser-cooled atomic cloud. Then, the trapping laser beam was turned off just before photoionization, and the excitation laser beam was turned on. Subsequently, the excitation laser beam was moved in the cavity until it overlapped with both the ionization laser beam and the ultracold atomic cloud. A good overlap was achieved by maximizing the measured shift in the resonance frequency of the cavity, induced by the ultracold plasma, at the moment of photoionization.

## B. Microwave cavity resonance spectroscopy

The shift in the resonance frequency  $\Delta\omega$  of the cavity was measured as a function of time  $t$  with the data-acquisition

system discussed in previous papers [16,17,19] and is related to the electron density of the ultracold plasma by [20]

$$\frac{\Delta\omega(t)}{\omega_0} = \frac{e^2}{2m_e\epsilon_0\omega_0^2}\bar{n}_e(t). \quad (9)$$

Here,  $\omega_0$  is the resonance frequency of the unperturbed cavity,  $e$  is the elementary charge,  $\epsilon_0$  is the vacuum permittivity,  $m_e$  is the electron mass, and the quantity  $\bar{n}_e$  is the field-averaged electron density, which is defined as

$$\bar{n}_e(t) \equiv \frac{\int_{V_{\text{cav}}} n_e(\mathbf{r}, t) |\mathbf{E}(\mathbf{r})|^2 d^3\mathbf{r}}{\int_{V_{\text{cav}}} |\mathbf{E}(\mathbf{r})|^2 d^3\mathbf{r}}, \quad (10)$$

with  $n_e$  being the local electron density at positions  $\mathbf{r}$  in the cavity;  $\mathbf{E}$  being the electric field of the used resonant eigenmode in the cavity, which is the  $\text{TM}_{010}$  mode in our case; and  $V_{\text{cav}}$  being the cavity volume.

Since the electric field is constant in the region  $V_p$  in the cavity where the ultracold plasma is created, i.e.,  $\mathbf{E}(\mathbf{r}) = E_0\hat{\mathbf{z}}$ , with  $E_0$  being the electric-field amplitude and  $\hat{\mathbf{z}}$  being the unit vector in the  $z$  direction, it can be taken out of the integral. This makes the field-averaged electron density at time  $t = \tau$  (the moment the plasma is created) a direct measure for the number of electrons in the cavity. Hence,

$$\bar{n}_e(\tau) = \frac{\int_{V_p} n_e(\mathbf{r}, \tau) |E_0\hat{\mathbf{z}}|^2 d^3\mathbf{r}}{\int_{V_{\text{cav}}} |\mathbf{E}(\mathbf{r})|^2 d^3\mathbf{r}} = CN_e(\tau). \quad (11)$$

Here,  $N_e$  is the total number of electrons in the plasma, and the constant  $C \equiv E_0^2 / \int_{V_{\text{cav}}} |\mathbf{E}(\mathbf{r})|^2 d^3\mathbf{r}$  is a proportionality constant that relates the field-averaged electron density to the number of electrons.

This basically makes the microwave cavity a charged-particle detector and therefore ideal for the measurements of the photoionization cross section using microwave cavity resonance spectroscopy in combination with the saturation technique.

However, in MCRS, the measured signal (field-averaged electron density) is related to the free electrons present in the plasma and not to the ions, as is the case in the saturation technique. To obtain a fit function that, in the case of MCRS, relates the measured signal to the pulse energy of the ionization laser and in addition takes the spatial profile of the ionization laser into account (as discussed in Sec. II), we rewrite Eq. (11) in terms of the ion density and use the expressions derived in Sec. II. Since the plasma is quasineutral, i.e.,  $n_e \approx n_i$ , the field-averaged electron density becomes

$$\bar{n}_e = CN_e \approx C \int_{V_p} n_i(\mathbf{r}) d^3\mathbf{r}, \quad (12)$$

with  $n_i$  being the ion density given by Eq. (6). Substitution into Eq. (12) yields

$$\bar{n}_e = C \int_{V_p} n_{\text{tot}}(0) \left[ 1 - \exp\left(-\frac{\sigma_{\text{pi}} F(x, z)}{2E_{\text{ph}}}\right) \right] dx dy dz. \quad (13)$$

The ionization laser in our experiment has a Gaussian beam profile and enters the cavity along the  $y$  direction (see Fig. 1). The fluence  $F$  of the ionization laser in Eq. (13) is therefore

given by

$$F(x, z) = \frac{E_{\text{pulse}}}{2\pi s_x s_z} \exp\left(-\frac{x^2}{2s_x^2} - \frac{z^2}{2s_z^2}\right), \quad (14)$$

with  $E_{\text{pulse}}$  being the pulse energy of a single ionization laser pulse and  $s_x$  and  $s_z$  being the rms sizes of the laser beam in the  $x$  and  $z$  directions of the cavity, respectively. The atomic density profile  $n_{\text{tot}}$  of the laser-cooled and trapped atoms in the magneto-optical trap is given by a Gaussian density profile as well:

$$n_{\text{tot}} = \frac{N_{\text{tot}}}{(2\pi)^{3/2} \sigma_x \sigma_y \sigma_z} \exp\left(-\frac{x^2}{2\sigma_x^2} - \frac{y^2}{2\sigma_y^2} - \frac{z^2}{2\sigma_z^2}\right), \quad (15)$$

with  $N_{\text{tot}}$  being the total number of atoms in the MOT before photoionization and  $\sigma_x$ ,  $\sigma_y$ , and  $\sigma_z$  being the rms sizes of the atomic cloud in the  $x$ ,  $y$ , and  $z$  directions, respectively.

Substituting the total atomic density profile [Eq. (15)] into Eq. (13) then gives

$$\bar{n}_e = \frac{CN_{\text{tot}}}{2\pi \sigma_x \sigma_z} \int_{-\infty}^{\infty} \int_{-\infty}^{\infty} \exp\left(-\frac{x^2}{2\sigma_x^2} - \frac{z^2}{2\sigma_z^2}\right) \times \left[ 1 - \exp\left(-\frac{\sigma_{\text{pi}} F(x, z)}{2E_{\text{ph}}}\right) \right] dx dz. \quad (16)$$

Here, we made use of  $\int_{-\infty}^{\infty} \exp(-y^2/2\sigma_y^2) dy = \sqrt{2\pi}\sigma_y$  since the ionization laser pulse propagates in the  $y$  direction and can therefore ionize excited atoms at all  $y$  positions along its path.

Equation (16) replaces the original fit function (8) used to determine the photoionization cross section; it takes the nonconstant fluence of the ionization laser beam into account and, since the atomic cloud is not much larger than the ionization laser beam size, the size of the atomic cloud as well. In the next section, this equation will be used to determine the photoionization cross section.

#### IV. RESULTS

We laser cooled and trapped a cloud of  $^{85}\text{Rb}$  atoms with, on average,  $\sim 3.4 \times 10^7$  atoms, and rms sizes  $\sigma_x = 0.8$  mm,  $\sigma_y = 0.6$  mm, and  $\sigma_z = 0.4$  mm. Subsequently, we photoionized the cloud, as discussed in the previous section; we turn off the trapping laser, wait for 1  $\mu\text{s}$  to let the atoms decay to the ground state, and then turn on the saturating excitation laser. After 250 ns from the start of the excitation laser pulse, we photoionize the atoms with the nanosecond laser. We measured the field-averaged electron density as a function of time for 10 different pulse energies of the nanosecond laser. In Fig. 2, the measured field-averaged electron density directly after photoionization is plotted as a function of the pulse energy for ultracold plasmas with four different initial electron temperatures: 50, 100, 200, and 500 K. The rf electric-field strength  $E_0$  in the cavity was set to  $E_0 \approx 0.5$  kV/m, except for the measurement of the plasma with an initial electron temperature of 500 K; in the latter case,  $E_0 \approx 1.0$  kV/m, which results in a better signal-to-noise ratio of the cavity's frequency shift and explains why the error bars on the data points in the 500-K graph in Fig. 2 are smaller than the rest.

From curve fitting the four measurements with Eq. (16), we found a cross section for photoionizing the  $5^2P_{3/2}(F' =$

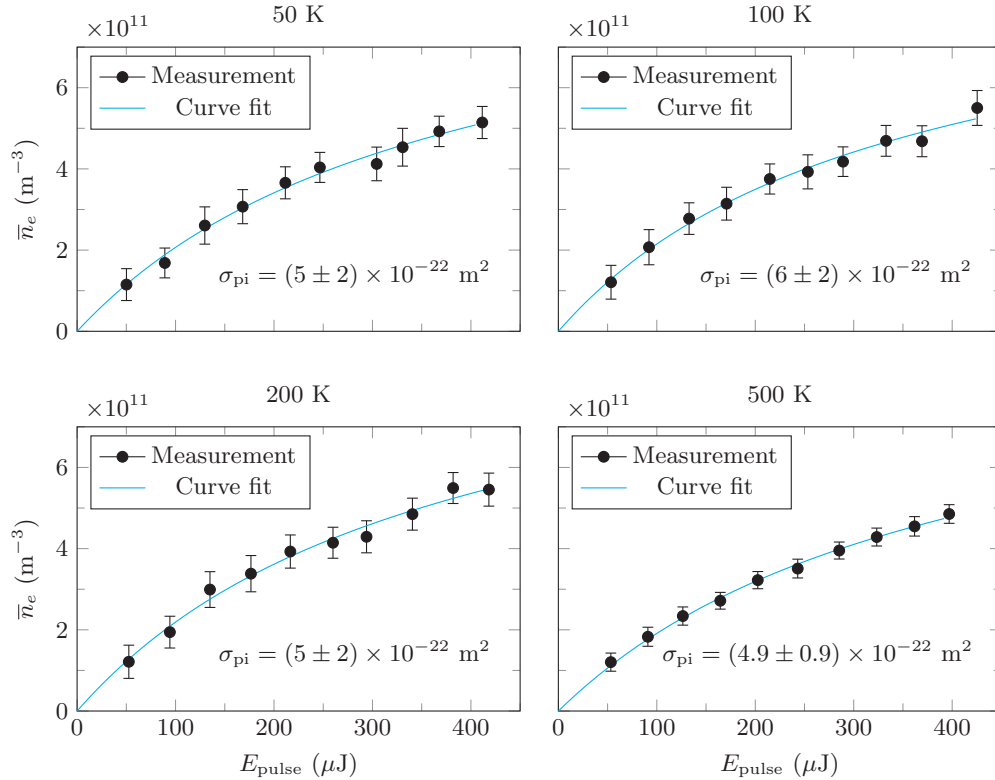


FIG. 2. Black dots: measured field-averaged electron density  $\bar{n}_e$  as a function of the pulse energy  $E_{\text{pulse}}$  of the nanosecond photoionization laser for ultracold plasmas with different initial electron temperatures. Blue curves: fits of the measured data using Eq. (16). The error bars in the 500-K graph are smaller than in the other graphs since the measurements were carried out for an rf electric-field strength  $E_0 \approx 1.0$  kV/m in the cavity, whereas  $E_0 \approx 0.5$  kV/m for the measurements of the other graphs.

4) excited state of  $^{85}\text{Rb}$  of  $(5 \pm 2) \times 10^{-22} \text{ m}^2$ ,  $(6 \pm 2) \times 10^{-22} \text{ m}^2$ ,  $(5 \pm 2) \times 10^{-22} \text{ m}^2$ , and  $(4.9 \pm 0.9) \times 10^{-22} \text{ m}^2$  for UCPs with initial electron temperatures of 50, 100, 200, and 500 K, respectively.

In comparison with theory and two earlier measurements performed by other groups, we find a cross section that is a factor of 2 to 3 lower. Regarding the theoretical value, to the best of our knowledge, the photoionization cross section has not been calculated for the  $5^2P_{3/2}(F' = 4)$  state, only for the  $5p$  state of  $^{85}\text{Rb}$ , which gives a cross section with a value between  $12.5 \times 10^{-22}$  and  $14 \times 10^{-22} \text{ m}^2$  at the ionization threshold, depending on the central-field model used [21]. This makes it difficult to quantitatively compare our measurement with the theoretical value, and therefore, the cross section should be calculated by taking the (hyper)fine structure of  $^{85}\text{Rb}$  into account.

Two earlier measurements performed for the photoionization cross section of the  $5^2P_{3/2}$  state, one with the MOT loading technique discussed in Sec. I and the other with the saturation technique on a collimated atomic beam, yielded values that are comparable with each other and are slightly higher than the theoretical value: Gabbanini *et al.* found a cross section of  $14.8(22) \times 10^{-22} \text{ m}^2$  with the MOT loading technique [7], while Nadeem and Haq reported a cross section of  $15 \times 10^{-22} \text{ m}^2$  with the saturation technique, with a total uncertainty of 16% [22].

## V. DISCUSSION DISCREPANCY

Potential sources of error in our measurements that could lead to a lower value for the photoionization cross section than in earlier measurements are a slightly detuned excitation laser beam, a larger photoionization beam area than expected, the tails of the Gaussian laser-cooled atomic cloud not being completely saturated due to the finite size of the excitation laser beam, and losses of atoms to the  $5^2S_{1/2}(F = 2)$  ground state due to the absence of a repump laser beam during the excitation of atoms. Below we estimate the error for each of those causes, and we find that their individual influence on the photoionization cross section is rather small ( $\leq 28\%$ ).

First, the excitation laser might, in practice, have a small detuning due to a mismatch between the frequency where we lock the laser and the  $5^2S_{1/2}(F = 3)$  to  $5^2P_{3/2}(F' = 4)$  atomic transition frequency. This could decrease the excited-state fraction  $f_2$ . However, the laser is typically locked within one natural linewidth  $\Gamma$  of the atomic transition, so we estimate  $f_2$  to be at least  $f_2 = \frac{1}{2}s_0/(1 + s_0 + 4\delta^2/\Gamma^2) \approx 0.47$ , with  $\delta$  being the laser detuning with respect to the transition,  $\Gamma/2\pi = 6.07$  MHz being the natural linewidth of the  $D_2$  line transition of  $^{85}\text{Rb}$  [18], and  $s_0 = 7 \times 10^1$  as discussed in Sec. III. Replacing the factor of  $\frac{1}{2}$  in the exponential of the fit function [Eq. (16)] by 0.47 therefore leads to a maximum increase of the photoionization cross section by  $\sim 7\%$ .

Second, a difference in the optical path length from the nonpolarizing BS cube (labeled 23 in Fig. 1) to the center of the cavity (1) and from the same BS cube to the CCD of the photoionization camera (22) might lead to an underestimate of the photoionization laser beam area. However, we estimate the difference in the optical path length to be less than 1 cm. Since we use a positive lens (21) with a long focal length of 25 cm to decrease the beam size of the photoionization laser, the beam area does not change considerably along its typical  $4\sigma_y = 2.4$ -mm path through the atomic laser-cooled cloud and changes by maximally 28% along a 1-cm optical path difference (for comparison, the Rayleigh length is 1.7 cm). Hence, this will lead to a maximally 28% higher cross section.

Third, since the excitation laser beam size is comparable to the size of the laser-cooled atomic gas cloud, the fraction of atoms in the excited state at the tails of the Gaussian atomic density distribution is less than  $\frac{1}{2}$ . To estimate the influence on the photoionization cross section, we can correct for this again by replacing the factor of  $\frac{1}{2}$  in the exponential of the fit function [Eq. (16)] by the excited state fraction  $f_2 = \frac{1}{2}s_0(\mathbf{r})/[s_0(\mathbf{r}) + 1]$  as a function of position, with  $s_0(\mathbf{r}) = I_{\text{exc}}(\mathbf{r})/I_{\text{sat}}$  being the earlier defined on-resonance saturation parameter and

$$I_{\text{exc}}(\mathbf{r}) = \frac{P}{2\pi\zeta_y\zeta_z} \exp\left(-\frac{y^2}{2\zeta_y^2} - \frac{z^2}{2\zeta_z^2}\right) \quad (17)$$

being the spatial intensity profile of the excitation laser beam, with  $P$  being the peak power and  $\zeta_y$  and  $\zeta_z$  being the rms sizes of the laser beam, respectively. Performing the correction with the measured  $P = 1.3$  mW and  $\zeta_y = \zeta_z = 3 \times 10^2$   $\mu\text{m}$  leads to an  $\sim 20\%$  higher cross section, so the effect of the nonsaturated tails of the atomic cloud on the photoionization cross section is not very large.

Fourth, since the excitation laser beam does not contain sidebands for the repump transition, atoms could be lost to the  $5^2S_{1/2}(F=2)$  ground state due to off-resonant excitation of the  $5^2P_{3/2}(F'=3)$  state. However, for the given saturation parameter  $s_0 = 7 \times 10^1$ , the steady-state fraction of atoms in the  $F'=3$  excited state, which has a detuning  $\delta/2\pi = 120.64$  MHz with respect to the  $F'=4$  state [18], becomes only  $\frac{1}{2}s_0/(1 + s_0 + 4\delta^2/\Gamma^2) = 0.02$ . Suppose that, in a worst-case scenario, all atoms from the  $F'=3$  excited state decay to the  $F=2$  ground state during the 250 ns between the start of the excitation laser pulse and the start of the ionization laser pulse; then only  $0.02 \times (\Gamma/2\pi) \times 250$  ns = 3% of the atoms will be lost. The absence of a repump laser beam during the

excitation of atoms will therefore not significantly change the values found for the photoionization cross section.

Finally, the uncertainty in the wavelength of the photoionization laser and the stability of the other parameters in the fit function (16) seem to have a negligible effect on the photoionization cross section when correcting for this. Hence, for future experiments the earlier-mentioned effects should therefore be taken into consideration first when repeating a measurement.

## VI. CONCLUSIONS AND OUTLOOK

We have demonstrated microwave cavity resonance spectroscopy as a technique to measure the excited-state photoionization cross section of laser-cooled atoms. We used a diffraction-grating-based magneto-optical trap inside a cavity to laser cool and trap a cloud of  $^{85}\text{Rb}$  atoms and showed that, by creating an ultracold plasma with a saturating excitation laser beam and by varying the pulse energy of a pulsed dye laser until the dye laser beam transition is saturated as well, we could measure the photoionization cross section of the  $5^2P_{3/2}(F'=4)$  excited state of  $^{85}\text{Rb}$  to the continuum. The measurements give a cross section of  $\sim 5 \times 10^{-22}$  m<sup>2</sup> for initial electron temperatures of 50, 100, 200, and 500 K. The found cross sections are approximately a factor of 2 to 3 lower than the theoretical value for the  $5p$  state of  $^{85}\text{Rb}$  and two earlier measurements performed with different techniques.

We investigated several potential sources of error that, in our case, could lead to a lower value than reported before; however, we found that their individual influence on the total photoionization cross section is not very large. Nevertheless, their combined effect should be considered and reduced when repeating an experiment. In addition, since the cross section is known only for the  $5p$  state from the literature and not for the  $5^2P_{3/2}(F'=4)$  state, a completely proper comparison of our measurements with the theoretical predictions is not yet possible. A more extensive calculation should be performed that takes the (hyper)fine structure of  $^{85}\text{Rb}$  into account.

## ACKNOWLEDGMENTS

This project was financially supported by the Netherlands Organisation for Scientific Research (NWO) under Project No. 14651 and ASML. The authors would like to thank the group of Prof. Dr. Riis of the University of Strathclyde for supplying a diffraction grating chip for the experiments and H. van Doorn and E. Rietman for the invaluable technical support.

[1] M. Saleem, S. Hussain, and M. Baig, *Optik* **158**, 664 (2018).  
 [2] V. Saini, P. Kumar, V. Subrahmanyam, and S. Dixit, *J. Quant. Spectrosc. Radiat. Transfer* **224**, 361 (2019).  
 [3] J. Beckers, T. van de Ven, R. van der Horst, D. Astakhov, and V. Banine, *Appl. Sci.* **9**, 2827 (2019).  
 [4] T. C. Killian, S. Kulin, S. D. Bergeson, L. A. Orozco, C. Orzel, and S. L. Rolston, *Phys. Rev. Lett.* **83**, 4776 (1999).

[5] T. P. Dinneen, C. D. Wallace, K.-Y. N. Tan, and P. L. Gould, *Opt. Lett.* **17**, 1706 (1992).  
 [6] R. V. Ambartsumian, N. P. Furzikov, V. S. Letokhov, and A. A. Puresky, *Appl. Phys.* **9**, 335 (1976).  
 [7] C. Gabbanini, S. Gozzini, and A. Lucchesini, *Opt. Commun.* **141**, 25 (1997).  
 [8] A. Kallenbach, M. Kock, and G. Zierer, *Phys. Rev. A* **38**, 2356 (1988).



- [9] K. J. Nygaard, R. E. Hebner, J. D. Jones, and R. J. Corbin, *Phys. Rev. A* **12**, 1440 (1975).
- [10] Y. Sato, T. Hayaishi, Y. Itikawa, Y. Itoh, J. Murakami, T. Nagata, T. Sasaki, B. Sonntag, A. Yagishita, and M. Yoshino, *J. Phys. B* **18**, 225 (1985).
- [11] C. C. Nshii, M. Vangeleyn, J. P. Cotter, P. F. Griffin, E. A. Hinds, C. N. Ironside, P. See, A. G. Sinclair, E. Riis, and A. S. Arnold, *Nat. Nanotechnol.* **8**, 321 (2013).
- [12] J. P. McGilligan, P. F. Griffin, E. Riis, and A. S. Arnold, *J. Opt. Soc. Am. B* **33**, 1271 (2016).
- [13] C. E. Burkhardt, J. L. Libbert, J. Xu, J. J. Leventhal, and J. D. Kelley, *Phys. Rev. A* **38**, 5949 (1988).
- [14] M. A. W. van Nindhuijs, Ph.D. thesis, Eindhoven University of Technology, 2021.
- [15] W. Mende, K. Bartschat, and M. Kock, *J. Phys. B* **28**, 2385 (1995).
- [16] M. A. W. van Nindhuijs, K. A. Daamen, J. G. H. Franssen, J. Conway, B. Platier, J. Beckers, and O. J. Luiten, *Phys. Rev. A* **100**, 061801(R) (2019).
- [17] M. A. W. van Nindhuijs, K. A. Daamen, J. Beckers, and O. J. Luiten, *Rev. Sci. Instrum.* **92**, 013506 (2021).
- [18] D. A. Steck, Rubidium 85 D Line Data, available online at <http://steck.us/alkalidata> (revision 2.2.3,9 July 2021).
- [19] M. A. W. van Nindhuijs, J. Beckers, and O. J. Luiten, *New J. Phys.* **24**, 063022 (2022).
- [20] D. M. Pozar, *Microwave Engineering*, 4th ed. (Wiley, Hoboken, NJ, 2011).
- [21] M. Aymar, O. Robaux, and S. Wane, *J. Phys. B* **17**, 993 (1984).
- [22] A. Nadeem and S. U. Haq, *Phys. Rev. A* **83**, 063404 (2011).